Ice-Draft Profiling from Bottom-Mounted ADCP Data

ANDREY Y. SHCHERBINA, DANIEL L. RUDNICK, AND LYNNE D. TALLEY

Scripps Institution of Oceanography, University of California, San Diego, La Jolla, California

(Manuscript received 9 August 2004, in final form 29 December 2004)

ABSTRACT

The feasibility of ice-draft profiling using an upward-looking bottom-mounted acoustic Doppler current profiler (ADCP) is demonstrated. Ice draft is determined as the difference between the instrument depth, derived from high-accuracy pressure data, and the distance to the lower ice surface, determined by the ADCP echo travel time. Algorithms for the surface range estimate from the water-track echo intensity profiles, data quality control, and correction procedures have been developed. Sources of error in using an ADCP as an ice profiler were investigated using the models of sound signal propagation and reflection. The effects of atmospheric pressure changes, sound speed variation, finite instrument beamwidth, hardware signal processing, instrument tilt, beam misalignment, and vertical sensor offset are quantified. The developed algorithms are tested using the data from the winter-long ADCP deployment on the northwestern shelf of the Okhotsk Sea.

1. Introduction

The use of acoustic Doppler current profilers (ADCPs) for ice draft (thickness of the submerged ice part) measurement was first proposed by Visbeck and Fischer (1995). They suggested that a combination of an ADCP with a high-accuracy pressure sensor would enable simultaneous measurements of the water depth and the distance to the lower ice surface, allowing ice draft to be obtained as the difference of the two. A similar method is widely used in specialized ice profiling sonars (Melling 1998; Strass 1998), but it has heretofore not been implemented using ADCPs because sufficiently accurate pressure sensors had not been used.

A typical ADCP offers at least two methods of estimating the distance to the surface. First, a dedicated bottom-tracking mode of an ADCP can be used. In this mode, specially configured and processed pings are used to establish the range and the velocity of a reflective surface with a high accuracy (on the order of 0.1 m) (Gordon 1996). Second, the distance to the surface can be determined by postprocessing the echo amplitude profiles of regular ["water tracking" ("WT")] pings (Visbeck 2002). The vertical sampling of such profiles is typically quite coarse (2–8 m) compared to the expected variability of the ice surface. However, as shown by Visbeck and Fischer (1995), and in the present study, the surface reflection peak in the echo intensity is well defined even with such a relatively low resolution. As a result, fitting a theoretical curve to the shape of the peak has a potential of increasing the resolution of the surface location by utilizing the data in several neighboring depth bins. Additional averaging over the four ADCP beams and over time is expected to reduce the statistical error further. The present study explores and compares the performance of both bottom-tracking and water-tracking methods applied to estimating the distances to the water–air and water–ice interfaces. Additionally, the effects of sound scattering and signal processing that are relevant to the problem of correct surface location, as well as the steps necessary to account for such effects, are discussed.

We performed concurrent ADCP and bottom pressure measurements in 1999–2000 using bottom moorings during an Okhotsk Sea shelf polynya experiment. The primary reason for the experiment was to track water property and velocity changes at the site of formation of the densest ventilated water in the North Pacific (Shcherbina et al. 2004). For quantitative flux budgets, it would be useful to know how much ice

Corresponding author address: Andrey Shcherbina, Woods Hole Oceanographic Institution, Physical Oceanography Dept., MS#21, Woods Hole, MA 02543.
E-mail: ashcherbina@whoi.edu

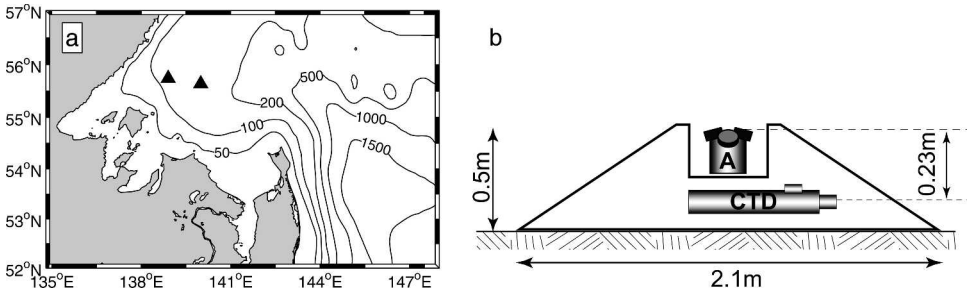

FIG. 1. (a) Map of the northwestern Okhotsk Sea showing the mooring location (triangles). (b) Schematics of bottom moorings, showing the relative locations of the upward-looking ADCP (A) and the CTD package within the conical hull of a mooring.

formed in the polynya, which involves tracking both the thickness and movement of the ice. The preferred in situ instrument for measuring ice thickness is the upward-looking ice profiling sonar (IPS) (Melling 1998), which uses a single vertical beam and has a higher vertical resolution (down to 1 cm) than the ADCP. However, these instruments could not be included in our experiment because of funding constraints. Therefore, we have attempted to reconstruct ice thickness from the ADCP information. Because the bottom-mounted instruments used in our experiment combined upward-looking ADCPs with high-accuracy pressure sensors and the added benefit of instrument stability, they were promising for this task. Section 2 below provides the information about the mooring equipment, and section 3 describes the algorithm of ice-draft estimation using ADCP data and correction procedures. Results of observations are shown in section 4.

2. Measurements and instrumentation

In a winter polynya study on the broad continental shelf in the northwestern Okhotsk Sea, two fixed bottom moorings ("landers") were deployed at 55°45′N, 138°54′E and 55°39′N, 140°00′E in 109 and 144 m of water, correspondingly (Fig. 1), and will be hereafter referred to as the "western" (shallower) and the "eastern" (deeper) ones. The landers were deployed in September 1999 and were recovered in June 2000 from the R/V *Professor Khromov*. The instruments were mounted in a fixed fiberglass hull (Fig. 1b) and, thus, were not subject to mooring motion. Each lander was equipped with an upward-looking RD Instruments (RDI) Workhorse 300-kHz broadband ADCP and a Paroscientific Digiquartz pressure sensor, the latter as part of a Sea-Bird Electronics SBE 16 SEACAT Recorder, which also performed temperature and conductivity measurements. Pressure, conductivity, and temperature were recorded with a 15-min sampling interval.

Each ADCP recorded the averages of 70 pings for each 16-min ensemble; the vertical bin size was 4 m. Both ADCPs operated in a "bottom tracking" ("BT") mode, which, in this case, measured the distance to and speed of ice using dedicated pings and signal processing that was different from that used for water velocity profiling. Three BT pings distributed among the regular (water tracking) pings of each 16-min ensemble were used.

The data from the shallower mooring will be used in the following sections to illustrate the algorithm of ice-draft estimation and data correction procedures. The results from both moorings are discussed in section 4.

3. Ice-draft profiling with ADCP

The thickness of the submerged part of ice sheet ("ice draft") can be deduced as the difference between the instrument depth H and the distance to the lower ice surface h (Fig. 2):

$$d = H - h. \tag{1}$$

As the water depth changes with tidal oscillations, the instantaneous depth is determined from the in situ water pressure P,

$$H = P/(g\bar{\rho}), \tag{2}$$

where g is the gravitational acceleration and $\bar{\rho}$ is the vertical average of water density. The mean density $\bar{\rho}$ was calculated using the density measured at the bottom and assumptions about the thermocline shape obtained from measured density profile and satellite observations of surface temperature [see section 3e(2)].

In our experiment setup, the ADCPs were used to determine the distance h to the surface based on the travel time of the sound reflected by the surface. Because of the high reflectivity of the interface, a typical echo amplitude profile exhibits a prominent peak near the surface (Fig. 3), so the distance to the surface can be

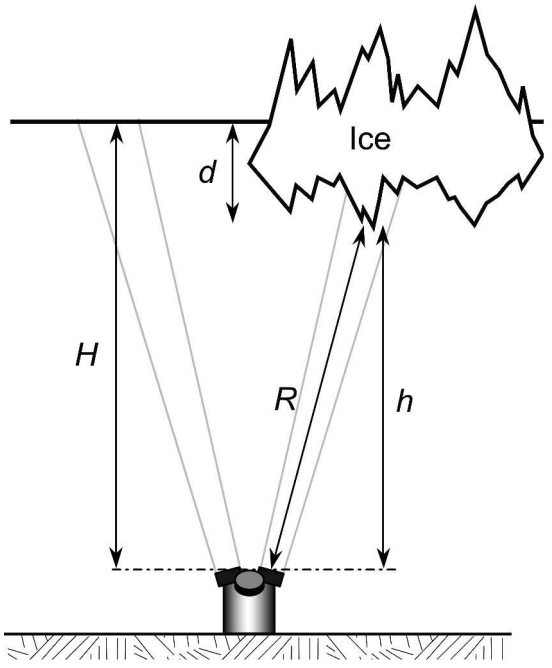

FIG. 2. Schematics of ADCP ice-draft profiling.

inferred from the location of the echo intensity maximum. However, the apparent location of this maximum is shifted relative to the true distance to the surface because of the combined effect of the fairly wide ADCP beam and the steep dependence of surface reflectivity on the incidence angle. Additional bias is introduced by the RDI ADCP signal-processing circuitry. Section 3a below details the effect of these factors on the shape and location of the surface maximum. The algorithms for the surface range estimate and quality control are described in sections 3b and 3c, and their performance is compared with the BT algorithm in section 3d. Section 3e outlines the correction procedures, designed to reduce the effects of changing atmospheric pressure, sound speed variation, beamwidth offset, and instrument misalignment on the ice-draft estimate.

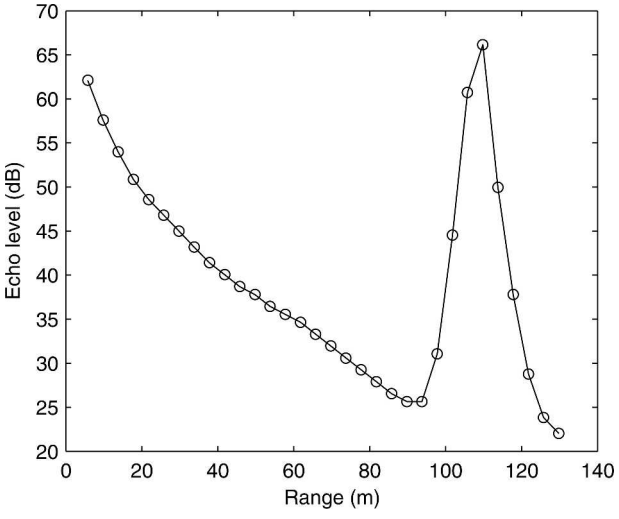

FIG. 3. Typical profile of ADCP echo level as a function of distance above the instrument. The decibel scale is based on the instrument's internal reference level. Water depth is approximately 110 m.

a. ADCP's surface echo formation

The echo intensity recorded by an ADCP is a result of a chain of the following processes: emission of a sound signal, its propagation through the water column, sound scattering from suspended particles and the surface interface, and, finally, the return signal acquisition and preprocessing. Among these processes, surface scattering [section 3a(1)] and signal preprocessing [section 3a(2)] are especially important for the problem of surface range estimation, because they control the location of the surface echo intensity peak.

1) SURFACE REFLECTION

Because of the finite width of an ADCP beam, it insonifies not a point but an ellipse on the water (ice) surface. The beamwidth of a 300-kHz RDI ADCP corresponds to a 8 m $\times$ 10 m footprint on a surface 100 m away from the instrument. The incidence angle within this ellipse varies from 18° to 22°. Coincidently, the scattering strength of the water surface changes most rapidly between 10° and 20° (Urick 1956), so the backscatter from the leading edge of the footprint (low incidence angle) is appreciably stronger than from the trailing edge. Additionally, the leading edge is located closer to the instrument, which leads to slightly lower attenuation of the sound reflected from it. As a result, the echo-level maximum shifts from the center of the ellipse (Fig. 4) (M. Visbeck 2004, personal communication). Consequently, the effective beam angle is less than the nominal one, and the inferred distance to the surface is biased low.

This effect can be illustrated with a simple model of reflection of an ADCP beam from an infinite horizontal rough plane. The level of the echo EL reflected from the surface at an angle θ from the vertical is (Urick 1975)

$$\mathrm{EL}(\theta) = \mathrm{SL} + \mathrm{TL} + S_s, \tag{3}$$

where SL is the source level, TL is the transmission loss, and S_s is the surface scattering strength (all expressed in decibels). (Volume backscattering has been neglected in this consideration.) We vary θ within $\pm 5°$ to form a cone around the ADCP beam axis, inclined at an angle

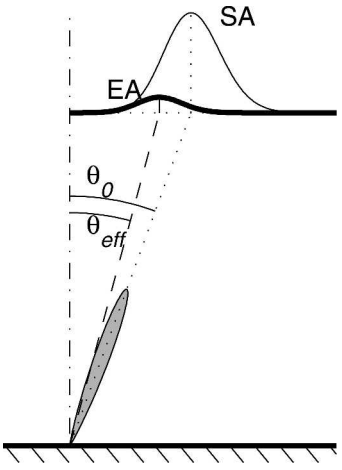

FIG. 4. Schematics of the beamwidth bias origination. Emission pattern of an ADCP beam (shaded) has a finite beamwidth, resulting in a relatively wide insonified footprint on the surface. Reflection from the inner edge of the footprint is stronger (see text for details), so the echo intensity distribution (EA) is shifted relative to the distribution of the incoming sound intensity (SA). As a result, the effective beam angle θ_{eff} is smaller than the nominal beam angle θ_0. Beamwidth is exaggerated by a factor of 2 for clarity, and the effect of sidelobes is neglected.

$\theta_0 = 20°$ to the vertical. We assume quadratic decay of the ADCP source level away from the beam axis, modeled as

$$\text{SL} = \text{SL}_0 - 3\frac{\Delta\theta^2}{\theta_{\text{hw}}^2}, \quad (4)$$

where $\Delta\theta$ is the angle measured from the axis of the beam, θ_{hw} is the beam half-width (2.2° for 300-kHz RDI ADCP), and SL_0 is an arbitrary constant. Following Gordon (1996), transmission loss is defined as

$$\text{TL} = -20\log_{10}(R) - 2\alpha R, \quad (5)$$

where $\alpha = 0.073$ dB m^{-1} is the absorption coefficient, $R = H/\cos(\theta)$ is the radial distance to the surface, and H is the instrument depth.

Surface scattering S_s varies greatly depending on surface roughness (Urick 1975), which is affected by wind conditions and presence of ice. For this model we use Chapman and Scott's (1964b) approximation, which is appropriate for young ice,

$$S_s = -10\log_{10}8\pi\eta^2 - 2.17\,\eta^{-2}\tan^{-2}(90° - \theta), \quad (6)$$

where η^2 is the mean square slope of the surface irregularities. For the open-water (OW) conditions, η^2 corresponds to the mean square slope of wind waves, which is related to the wind speed W using the empirical relationship (Cox and Munk 1954)

$$\eta^2 = 0.003 + 5.12 \times 10^{-3}W, \quad (7)$$

where W is expressed in meters per second. The model does not explicitly include the provisions for the tilt of the reflective surface on scales comparable to the size of the beam footprint, which may be present in older ice because of ridging and the formation of large keels. Variation of this large-scale tilt, combined with ensemble ping averaging performed by an ADCP, may change the shape of the observed echo intensity profile [see section 3a(3)]. Consideration of such tilt is equivalent to changing θ_0 and would have little influence on the effects illustrated by our simple model.

Distribution of the terms of Eq. (3) across the beam is shown in Fig. 5a for a typical wind speed of $W = 5$ m s^{-1} observed at the mooring location in autumn. It can be seen that the maximum echo level is achieved at an angle $\theta_{\text{eff}} = 19°$, which can be interpreted as an "effective beam angle." Because the echo from this angle arrives earlier than the one from the nominal beam angle, the distance to the surface is underestimated by 0.7 m compared to the true $H = 110$ m (0.6%). This effect becomes more pronounced as the reflection becomes more specular at a lower wind speed (Fig. 5b). At $W = 1$ m s^{-1} the bias in the range estimate reaches 1.73 m (1.6%). It should be noted that this bias is a result of inherent ADCP features—the 20° beam slant that leads to the maximum variation of surface scattering strength across the beam, which is also fairly wide. Both BT and WT range estimates are equally susceptible to this bias.

The model of the beamwidth bias is equally applicable to the ice-covered (IC) conditions, if an appropriate value of the mean square slope η^2 is substituted. The acoustic behavior of young sea ice is similar to that of the surface wave field generated by 7–10 m s^{-1} winds (Chapman and Scott 1964a; Macpherson 1963), and the mean square slope of the young ice can be approximated to the first order by substituting an appropriate W in (7).

The beamwidth bias may be the biggest obstacle in ADCP ice profiling, because it depends on ice roughness, which, in turn, may be correlated with the ice thickness. Consequently, the signals of ice roughness and thickness are likely to be aliased in the ADCP draft measurements. It appears to be impossible to separate these signals without external information about ice roughness. During the OW periods, this beamwidth bias is expected to have even greater variability in response to changes of surface roughness.

The above model is applicable for infinitely short pings. Broadband ADCPs use coded pulses with the duration τ almost equivalent to the vertical bin size ($\tau =$

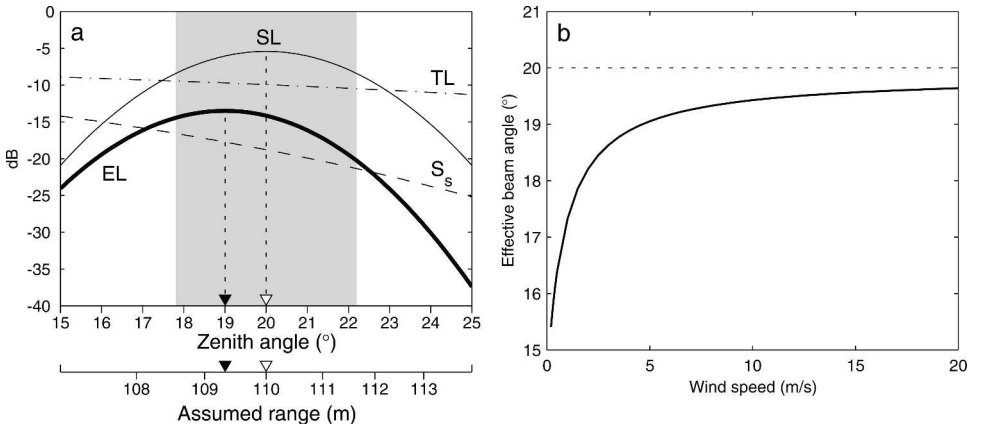

FIG. 5. Model of the beamwidth bias. (a) Distribution of SL, TL, S_s, and EL across the ADCP beam in meridional direction (arbitrary reference level). Beamwidth, defined by −3 dB drop in SL is shaded. The lower horizontal axis shows the range inferred from the echo return time. Nominal beam angle and true distance to the surface are marked by white triangles. Black triangles mark the effective beam angle, defined by the maximum echo level, and the corresponding (biased) range estimate. (b) Dependence of effective beam angle on wind speed (solid line). Nominal beam angle is shown by dashed line.

3.83 m in our case). As a result, the pulses overlap, so that the return echo time series is effectively smoothed with the rectangular window of length τ.

2) HARDWARE SIGNAL PROCESSING

An ADCP's primary purpose is accurate velocity measurement. Echo intensity profiling, on the other hand, is an ancillary task, intended chiefly for quality control. Consequently, the details of the echo signal preprocessing are rarely known or controlled. Unfortunately, some of the aspects of such preprocessing lead to a significant shift of the surface peak.

A time series of echo intensity is obtained by the ADCP's return signal strength indicator (RSSI) circuit. Time t elapsed between the ping start and arrival of an echo can be converted to the vertical distance (range) to the echo origin as $h = 0.5ct \cos \theta_0$, where c is the sound speed and θ_0 is the nominal beam angle. Consequently, the time series of echo intensity can be interchangeably interpreted as functions of range. Similarly, the temporal parameters, such as pulse length, are commonly expressed in units of length, implicitly implying such equivalence.

According to RDI (P. Spain 2004, personal communication), the raw RSSI output is passed through a low-pass RC filter, which performance can be modeled as

$$W(\tau) = \exp(-\tau/\tau_{RC}), \tag{8}$$

where τ_{RC} is a time constant equivalent to 25%–50% of the bin length. The exact value of the time constant is determined by the hardware based on the chosen bin length, but it is not reported to the firmware and should be assumed unknown. Because the filter is strongly asymmetric, the surface peak is shifted forward in time, and, consequently, in range (Fig. 6). The amount of shift of the maximum echo intensity depends on τ_{RC} and the shape of the original peak, and ranges from zero, for a delta function, to approximately $1.96\tau_{RC}$, for a wide Gaussian peak. For $\tau_{RC} = 2$ m and the shape of

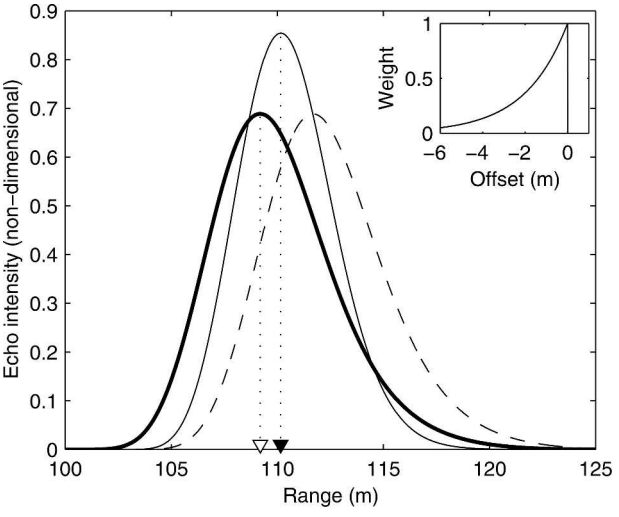

FIG. 6. Illustration of the effects of echo amplitude signal processing on hypothetic raw echo intensity signal (thin solid line). Results of low-pass filter application (dashed line) and subsequent shift (thick line) are shown. Time axis is converted to range for convenience. Black and white triangles show the locations of the maxima or the raw and processed signal, respectively. Inset shows the distribution of weights of RC filter ($\tau_{RC} = 2$ m), applied to the signal.

the peak modeled in section 3a(1), the shift is on the order of 1.5 m.

The filtered time series is then sampled near the *end* of the time gate corresponding to a given vertical bin (more precisely, with a delay of broadband code lag λ *after* the end of a gate), and the obtained value is assigned to the *middle* of the bin. Consequently, the peak is effectively shifted backward in time and range by $\Delta h = 0.5\tau_{BL} + \lambda$, where τ_{BL} is the bin length. In our case, $\tau_{BL} = 4$ m and $\lambda = 0.48$ m, giving $\Delta h = 2.48$ m. Overall, as a result of signal processing alone, the surface peak in the echo amplitude is shifted approximately 0.98 m closer to the instrument (Fig. 6). Unlike the surface reflection bias, the signal-processing shift of the peak is independent of water depth.

We investigated a possibility of the reversal of the effect of the RC filter on the echo intensity record. However, poor knowledge of the filter time constant and sparse sampling of the surface echo peak makes such reversal unfeasible. Consequently, we acknowledge the existence of the signal-processing bias without attempting to correct it.

3) Ensemble averaging and background noise

In the simple model considered in the previous sections, the echo intensity rapidly falls off to zero outside of the surface peak (Fig. 5). In reality, however, the minimum echo level is set by volume backscattering and internal system noise. For the RDI ADCP used in our experiment this background level was on the order of 20 dB (relative to the unknown instrument reference), as can be seen from a typical echo-level profile (Fig. 3). Consequently, a "Ω"-shaped curve (Fig. 7, dashed line) is a more realistic model of the amplitude of ADCP ping surface echo.

Each echo intensity profile that is recorded by the ADCP represents an average of many surface peak realizations (70 in our case) acquired over the ensemble interval. Both the location and the angle of scattering surface vary considerably over the duration of an ensemble (16 min, in our case). During the open-water conditions, this variability is primarily the result of surface wave activity. Advection of the jagged lower ice surface through the ADCP beam leads to similar quasi-random variability during the ice-covered periods. (At a typical ice speed of 0.2 m s^{-1} observed during this deployment, each ensemble represents a 200-m section of under-ice topography.) Consequently, the recorded echo intensity curve is a convolution of a single-ping profile as modeled above and a probability distribution of surface height. For normally distributed surface height, the ensemble averaging of the individual single-ping echo intensity profiles that are cut off at the background noise level results in a bell-shaped profile of the surface maximum (Fig. 7).

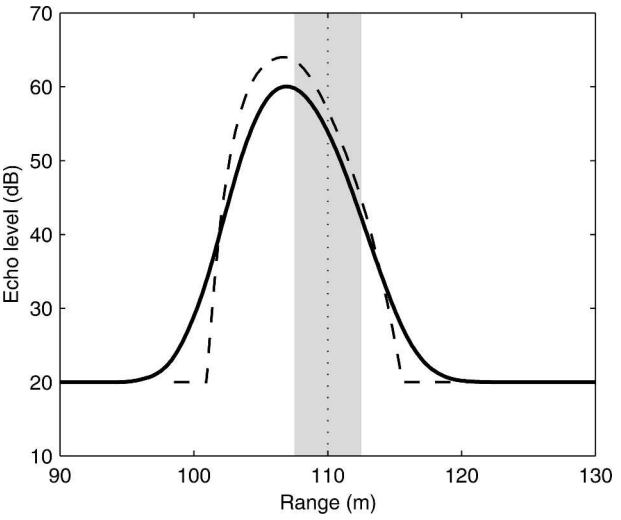

FIG. 7. Illustration of the effect of ensemble averaging in presence of background noise and surface variability. Modeled single-ping echo-level profile is shown by dashed line. Solid line represents an average of an ensemble of pings reflected from randomly varying surface. Vertical dotted line marks the mean surface location (110 m); gray shading represents one standard deviation (± 2.5 m). Noise level is set at 20 dB (arbitrary reference level).

b. Determining location of the surface peak

The shape of the echo-level peak associated with the surface can be approximated by combining the models of surface reflection and signal processing discussed above. The two most important features of the surface peak are its skewness and a prominent shift (up to several meters) relative to the true surface range. With the judicious choice of model parameters (source level, beamwidth, DSP constants, surface roughness and variability, etc.), the modeled shape of the surface peak agrees well with the observed ADCP echo intensity profile (Fig. 8).

Ideally, the distance to the surface and other model parameters can be estimated by fitting the model curves to the observed echo-level data. However, even in a simple model these parameters control subtle changes of the shape of the peak, so accurate parameter estimation is not possible, given the coarse vertical resolution used in our experiment. Instead, a modified Gaussian profile was used to approximate the surface peak profile $A(z)$:

$$A(z) = a_0 \exp\left[-\left(\frac{z - h_0}{\delta}\right)^2\right] + a_1 z + a_2, \qquad (9)$$

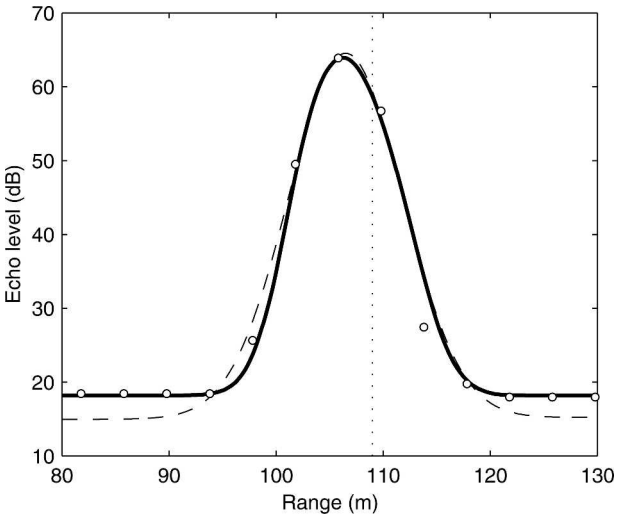

FIG. 8. Comparison of the modeled shape of the near-surface echo-level profile (thick line) with the observed (circles). Model parameters (source level, water depth, surface roughness and variability) were subjectively adjusted for the best fit. Vertical dotted line marks the water depth used in the model. Modified Gaussian fit is shown by dashed line. Decibel scale is based on the instrument's internal reference level.

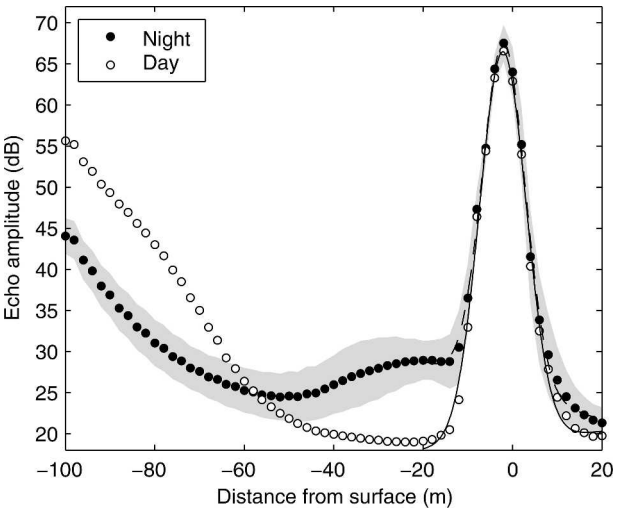

FIG. 9. Influence of near-surface plankton congregation on the vertical structure of echo amplitude. Profiles of echo amplitude at night- (plankton up, solid circles) and daytime (plankton down, open circles) are shown. One standard deviation is shown by gray shading. Thin lines show modified Gaussian approximation of the peak shape, fitted to the data using least squares. Decibel scale is based on the instrument's internal reference level.

where parameters a_0, a_1, a_2, h_0, and δ were obtained by the least squares fit of (9) to the 11 points of each amplitude profile in the vicinity of the expected peak (Fig. 8). A weighted least squares algorithm was used, with the weights of the data points proportional to the squares of the echo amplitudes, so that the values close to the maximum influence the fit more than the "tails." The linear term in (9) allows for echo amplitude changes caused by zooplankton congregation near the surface at night (mostly during the ice-free periods), which brings a substantial periodic increase of the echo amplitude just below the surface (Fig. 9). The fitted value of h_0 should be considered as an estimate of the mean instrument to surface distance over the ensemble duration.

It is important to mention that the vertical coordinates z_i of the ADCP bins may vary from ping to ping. The reason for this variation is the changes in the effective length of the transmit pulse with changing sound speed. {Note that this effect should be distinguished from the effect of changes in pulse travel time that are also caused by sound speed variation [see section 3e(3)].} For most ADCP applications, the vertical bin coordinates are retrieved once at the beginning of the record and are assumed to be constant. However, for the purpose of the surface range estimate the vertical bin coordinates should be computed for each ping separately to account for changing pulse length. In our case the position of the first bin varied by as much as 15 cm.

We understand that the modified Gaussian function is not an accurate approximation of the surface peak shape, which is markedly asymmetric (Fig. 8). Fitting a modified Gaussian shape (9) is, however, superior to a simple maximum search based on polynomial interpolation. Compared to the latter, our method provides not only the estimate for the instrument to surface distance h_0, but also information about the width δ of the surface maximum and a standard deviation σ of the data from the fit, which can be used for quality control of the estimate of h, as described in the next section.

c. *Filtering the WT signal*

The fit (9) provides a variety of information about the shape of the surface maximum: location (h_0), height (a_0), and width (δ) of the peak, and the misfit (σ) between the data and a modified Gaussian model (9). These parameters can be used for filtering out the spurious range detections caused by unexpected surface reflection pattern. The peak characteristics may depend on the presence of ice at the surface, so the filtering parameters should be determined separately for IC and OW situations.

The presence of surface ice cover influences a wide range of the ADCP return signal parameters in addition to the echo amplitude, namely, the correlation of surface reflection, and near-surface variances of horizontal, vertical, and error velocities (Visbeck and Fis-

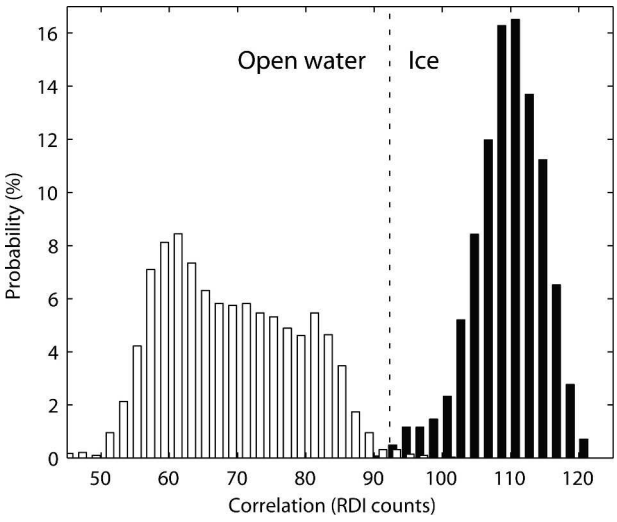

FIG. 10. Distribution of ADCP signal correlation during definitely open water (15 Oct–15 Nov, open bars) and definitely ice covered (15 Feb–15 Mar, filled bars) periods. Vertical dotted line shows the threshold value C_{ice}. Data from the first bin above the mean sea surface level are shown.

cher 1995). It was empirically established that the value of signal correlation in the first bin above the mean surface level yields the most reliable detection of ice presence in our configuration, because its distributions for "definitely IC" (15 February–15 March) and "definitely OW" (15 October–15 November) exhibit the clearest separation (Fig. 10). The critical value of correlation $C_{ice} = 92.3$ optimally separates the two distributions, so that over 99.9% of correlation during the definitely IC period was higher than C_{ice}. Similarly, over 99.3% of correlation during the definitely OW period was lower than C_{ice}. Consequently, we assume that the surface ice is present whenever the signal correlation exceeded C_{ice}. Such ice detection also shows a good agreement with the Special Sensor Microwave Imager (SSM/I) ice observations; correlation between the daily ice cover fractions that were determined with the two methods was 93%.

The distributions of the surface peak width and height, determined by a modified Gaussian profile fitting, are noticeably different for the IC and OW periods that are distinguished using the ADCP signal correlation criterion (Fig. 11). Median values of the surface peak width δ were 5.7 and 7.2 m for IC and OW conditions, correspondingly. The median values of peak height were 39 and 46 dB, correspondingly.

Anomalously narrow and low surface peaks, occurring predominantly during the OW periods, likely indicate instances of specular reflection at the surface associated with calm conditions. In such conditions, the return of the main lobe of the signal can be greatly reduced, and the surface peak is largely the result of sidelobe scattering. Consequently, the range that is estimated from such a peak is likely to be biased low, and, thus, should be excluded from the analysis. At the same time, an anomalously wide surface peak may be the result of enhanced subsurface scattering that is caused by plankton congregation, and should also be excluded. Retaining only values within one standard deviation of the median value of the peak width and within two standard deviations of the median value of the peak height, provided a reasonable balance of valid and false outlier detection. Additionally, range estimates that are associated with a high misfit between the observed echo amplitude data and modified Gaussian profile (9) should also be disregarded. An example of the effect of filtering on WT range estimates is shown in Fig. 12. On average, approximately 17%, 6%, and 11% of the data were rejected by peak width, peak height, and misfit criteria, correspondingly. The rejection rate was the highest (over 60%) during the spring melt, which was likely a result of the greater variability of surface conditions.

d. Comparison of WT and BT

Surface range h can also be obtained using the BT mode of an ADCP. In this mode, the ADCP periodically emits specially configured bottom-tracking pings, which are processed by the firmware to determine the location of the surface maximum of echo intensity. In the BT mode the echo time series is sampled more frequently compared to the WT mode (Gordon 1996). The BT range, which is approximately twice the distance to the surface, is subdivided into as many as 200 depth bins, giving a vertical resolution of about 1.3–1.5 m for our case. However, the interpolation of the surface peak position is neither performed, nor is it possible in postprocessing, because no raw data are recorded in the BT mode.

On the other hand, even though the vertical resolution of the raw WT echo amplitude is lower (4 m in our case), fitting the shape of the surface peak, described in section 3b, results in a better resolution than that of the BT method. The additional advantage of the WT method of surface range estimation over BT is its ability to measure the distance not only to the ice surface, but to the water–air interface as well. The distances from the instrument to the open-water surface obtained using the WT method aid the calibration of ice-draft estimates [see sections 3e(3) and 3e(4)].

The ADCPs used in our moorings were among the first self-contained units to record bottom-tracking information. As a result, a direct comparison of the BT and WT methods of surface ranging is possible during

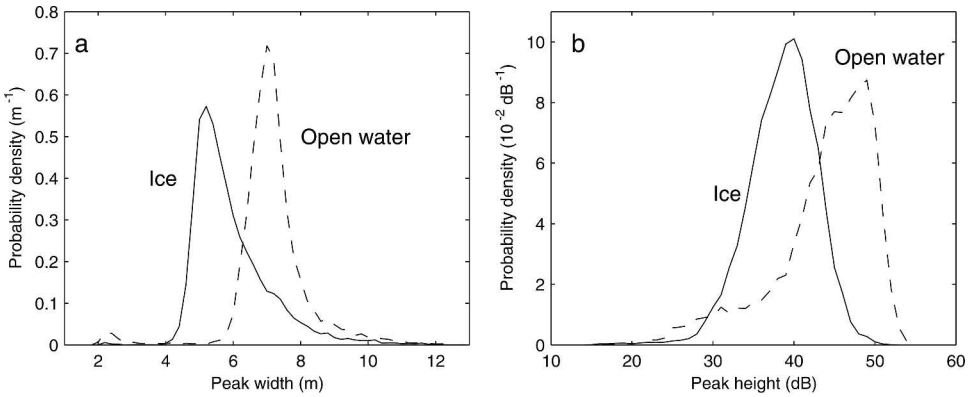

FIG. 11. Distribution of (a) the width and (b) the height of the surface peak for ice-covered (solid line) and open-water (dashed line) conditions. Ice detection is based on echo correlation.

the ice-covered period (January–May). In general, the two methods of range estimation agreed over a wide range of temporal scales (Fig. 13), with squared coherence over 0.75 (significant at over 85%) in the subtidal frequency range (Fig. 13b). For the most energetic tidal bands, the squared coherence reached 0.98. The noise level at time scales shorter than 6 h was noticeably higher in the BT record. At the highest resolvable frequency, the noise energy of the BT range estimate exceeded that of the WT estimate by a factor of 3. The mean difference between the raw unfiltered WT and BT range estimates was 14 cm (0.13%). The filtering described in the previous section reduces this difference to 10 cm, which is still statistically significant.

The variance of the ADCP range estimate exceeded that of the pressure-derived depth by a factor of 5 in the subtidal band, and up to a factor of a 100 at higher frequencies (Fig. 13a). On the other hand, energies in the tidal bands that were obtained with all three methods were identical. Higher variance of the ADCP range estimate can be explained by a number of surface factors not reflected in the bottom pressure record. Ice cover topography is obviously one of such factors. Others may include short-period surface waves, whose

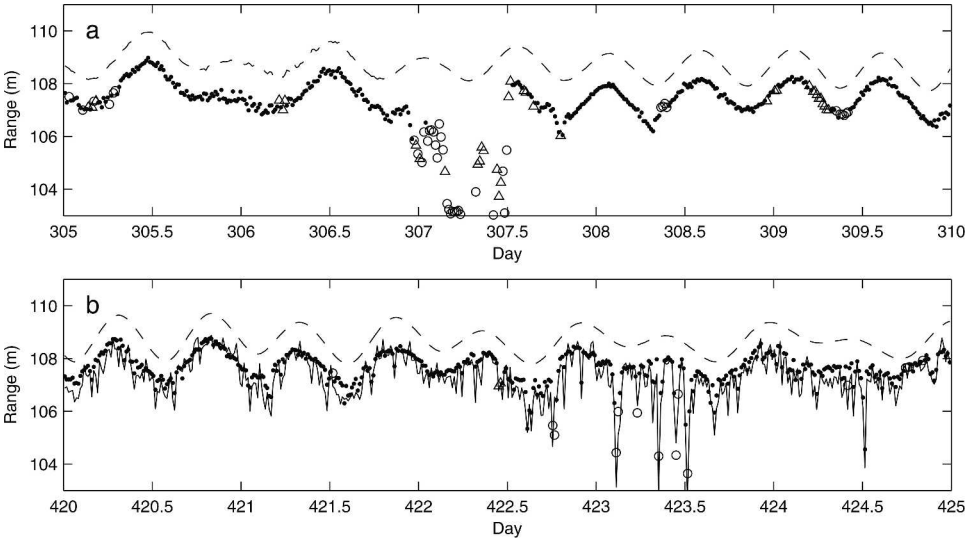

FIG. 12. Performance of the WT surface detection algorithm in (a) open-water (2–7 Nov 1999) and (b) ice-covered (25 Feb–1 Mar 2000) conditions, compared to range estimate based on bottom pressure (dashed line). Black dots mark the useable range estimates, and open symbols represent the values discarded based on peak width (open circles), peak height (open triangles), and misfit (open squares) criteria. The BT range estimates are shown by the thin solid line when available (only in ice-covered conditions). Raw uncorrected data of beam 1 are shown.

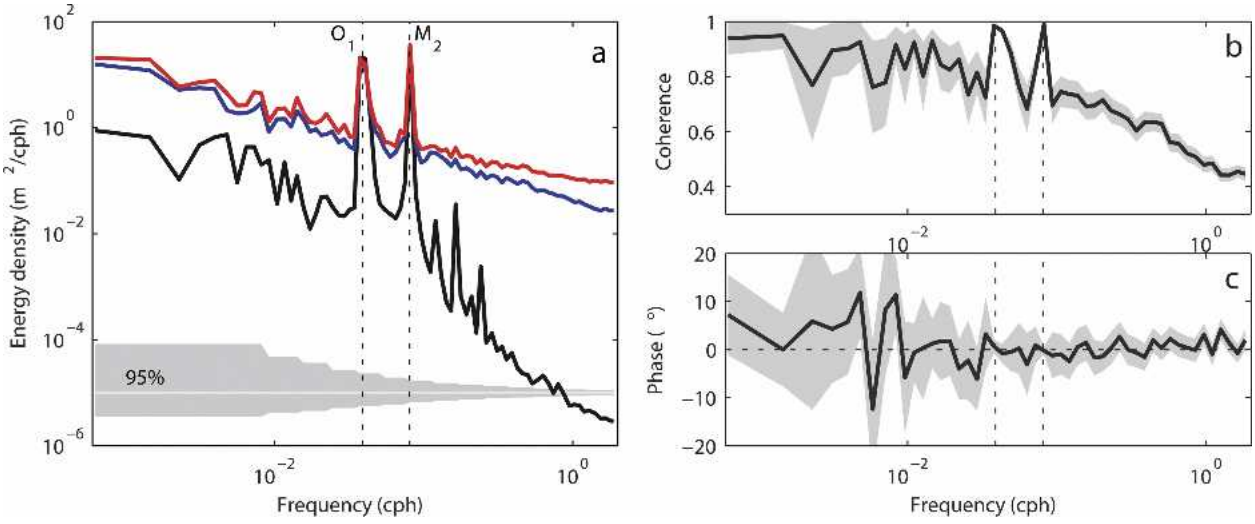

FIG. 13. (a) Power spectra of wintertime (Jan–May) range estimates based on pressure (black), water-track (blue) and bottom-track (red) data. (b) Squared coherence and (c) phase of the bottom-track and water-track range estimates over the same period; 95% confidence intervals (shading) and two major tidal frequencies (vertical dashed lines) are shown.

pressure signature decays significantly with depth, as well as variation of surface scattering, which introduces a variable bias in ADCP surface ranging [see section 3e(3)].

We conclude that the quality of the WT and BT range estimates are comparable, and the ice-profiling technique described herein can be performed with installations lacking BT capabilities as well. With the BT mode enabled (as in our setup), each ADCP ensemble provides eight independent estimates of range *h,* which can be used to improve the statistical stability of the ice-draft estimate.

e. Corrections and errors

The ice draft is estimated as a difference between the water depth that is derived from the bottom pressure and the distance to the ice surface, measured by the ADCP (1). Each of these distances is several orders of magnitude greater than the expected ice draft, so even small errors in either of the range measurements drastically affect the accuracy of the resulting ice-draft estimate. Consequently, the influence of the external factors on the right-hand side terms of (1) should be eliminated as accurately as possible.

An offset of over 1 m between the raw range estimates based on ADCP and pressure data can be seen even during the OW conditions, when it cannot be explained by the ice presence (Fig. 12a). Several factors are expected to contribute to this offset. Sound speed variations throughout the thermocline are a major uncertainty that can potentially lead to a few percent error in ADCP range estimates, which translates to a few meters over a 100-m range. As was shown in sections 3a(1) and 3a(2), substantial range biases (>1%) can also result from a finite width of the ADCP beam and the signal-preprocessing procedures. The pressure record is affected by atmospheric pressure changes typically corresponding to a depth offset of a fraction of a meter. Additionally, the instrument tilt, misalignment, and sensor separation can also contribute to the difference between the range estimates. The following sections quantify the effects of these factors on the range estimate and outline the procedures used to eliminate or reduce them.

1) PRESSURE CORRECTIONS

The Digiquartz pressure transducer has an accuracy of 0.01% (1 cm at 100 m). It was calibrated before and after the cruise. The difference between the two calibrations of the pressure sensor was low (0.04%). We distributed the correction linearly throughout the record.

According to the National Centers for Environmental Prediction (NCEP) meteorological reanalysis, atmospheric pressure at the mooring site varied with an amplitude of about 0.2 db (corresponding to 20 cm of surface height). This variability was removed from the bottom pressure data before calculation of depth *H*. Time series of 4-times-daily NCEP sea level pressure interpolated to the location of the moorings were used.

The instruments were activated several weeks before the deployment. Consequently, the pressure record that

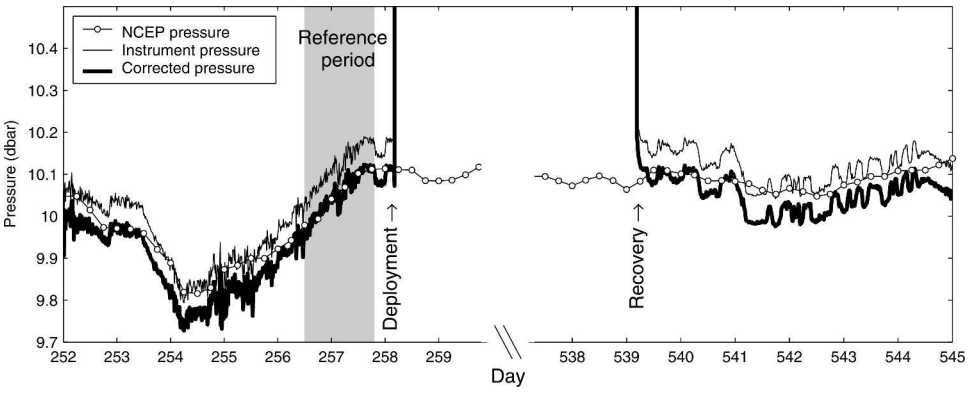

FIG. 14. Pressure sensor surface calibration. NCEP reanalysis sea level pressure interpolated at the site of the mooring (open circles), raw pressure record (thin black line), and corrected pressure (thick black line) are shown. Reference period over which the offset was calculated is shown by gray shading. Periods before deployment and after recovery are shown. Significant deviation of the corrected pressure from NCEP record before day 256 and after day 541 may be the result of the geographical separation of the instrument from the mooring site onto which NCEP data were interpolated.

is measured by the instruments on deck prior to deployment can be matched with the NCEP data to eliminate the systematic difference between these datasets (Fig. 14). The mean offset between the two records over a period of 1 day before the deployment was on the order of 0.1 db (10 cm of water column). This was subtracted from the measured bottom pressure data. Time series of measured pressure corrected this way coincided well with the NCEP record after the instruments were recovered (Fig. 14), suggesting that neither record drifted significantly over the 9-month deployment period.

2) SOUND SPEED CORRECTIONS

The BT range, as well as the WT bin positions, reported by the instrument is calculated using the speed of sound c_{ADCP} based on the data of the instrument's low-accuracy temperature sensor and fixed salinity. A more accurate estimate of sound speed at the bottom c_b was obtained using the CTD record of bottom temperature and salinity (Fig. 15). The difference between c_b and c_{ADCP} was generally less than 1.5 m s^{-1} (0.1%).

More importantly, the temperature and salinity changes in the thermocline lead to the vertical variation of sound speed by almost 2% (Fig. 16). The situation is further complicated by seasonal changes of the surface layer temperature, which are evident from the satellite observations of sea surface temperature (Fig. 17). Vertical temperature and salinity profiles were measured before the deployment (Fig. 16a), but not during the experiment. We assume that the general shape of these profiles remained invariant during the experiment, but that the thermocline became less pronounced as the surface cooling progressed. A time-varying "thermocline strength" factor r can be derived as

$$r(t) = \frac{T_s(t) - T_b(t)}{T_{s,0} - T_{b,0}}, \tag{10}$$

where $T_b(t)$ is the bottom temperature measured by the mooring's CTD; $T_s(t)$ is the surface temperature, approximated by an exponential fit of the satellite SST data (Fig. 17); and $T_{b,0}$ and $T_{s,0}$ are the bottom and surface temperatures, measured during the predeployment survey. Evolution of the vertical profiles of water properties can then be approximated as follows [using the temperature profile $T(z, t)$ as an example]:

$$T(z, t) = T_b(t) + r(t)[T_0(z) - T_{b,0}]. \tag{11}$$

Several profiles of sound speed that are calculated from temperature and salinity profiles approximated using (11), are shown in Fig. 16b. Even though this is just a model, it captures the gradual erosion of the warm surface layer, which is presumably the predominant feature.

Once the vertical sound speed profiles $c(z)$ have been reconstructed, the original ADCP range estimates h can be corrected,

$$h_c = (c_{\mathrm{eff}}/c_{\mathrm{ADCP}})h_p, \tag{12}$$

where h_p is the surface range corrected for the signal-preprocessing bias as described in the previous section, h_c is the surface range that is additionally corrected for

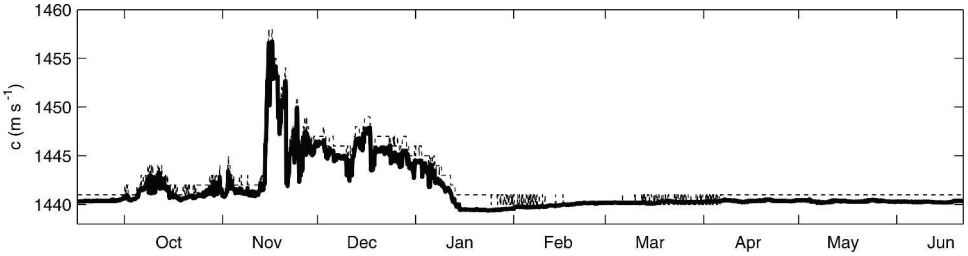

FIG. 15. Sound speed reported by ADCP (c_{ADCP}, dashed line) and calculated using the measured temperature and salinity (c_b, thick solid line).

sound speed variations, and c_{eff} is the effective sound speed given by

$$c_{\mathrm{eff}} = H\left[\int_0^H c(z)^{-1}\,dz\right]^{-1}. \tag{13}$$

Because the sound speed varies only by a few percent, we can expand it about its bottom value c_b: $c = c_b + c'$, where c' is a small depth-dependent correction. Then,

$$\begin{aligned} c_{\mathrm{eff}} &= H\left(\int_0^H (c_b + c')^{-1}\,dz\right)^{-1} \\ &\approx c_b H\left(\int_0^H \left(1 - \frac{c'}{c_b}\right) dz\right)^{-1} \\ &= c_b\left(1 - \frac{\overline{c'}}{c_b}\right)^{-1} \approx c_b + \overline{c'} = \overline{c}, \end{aligned} \tag{14}$$

where the overbar denotes a vertical average, so that $\overline{c} = (\int[c(z)\,dz]/H)$. Consequently, a simple mean vertical sound speed $\overline{c}$ can be used instead of the harmonic mean (13). The inaccuracy of such substitution for a typical sound speed profile (Fig. 16b) is less than 0.1 m s^{-1} (<0.01%).

The effective sound speed obtained from (10), (11), and (14) differs from c_b by less than 0.5% (Fig. 18). This value is based on a relatively crude first-guess assumption of a constant mixed layer depth. The uncertainty of c_{eff}, resulting from such an assumption, can be estimated by considering two extreme cases: the bottom value of sound speed c_b extending to the surface (no mixed layer), and the surface value c_s extending to the bottom (deep mixed layer). The effective sound speed is consequently expected to lie between c_b and c_s, so that its maximum deviation from c_b is less than 2% (Fig. 18). The effects of changing the mixed layer depth are not addressed in this study because of the lack of water column data. It should be noted that in winter, when the water column is homogeneous, sound speed at the surface is 0.13% lower than at the bottom because of the pressure effects (Fig. 18). However, because in this

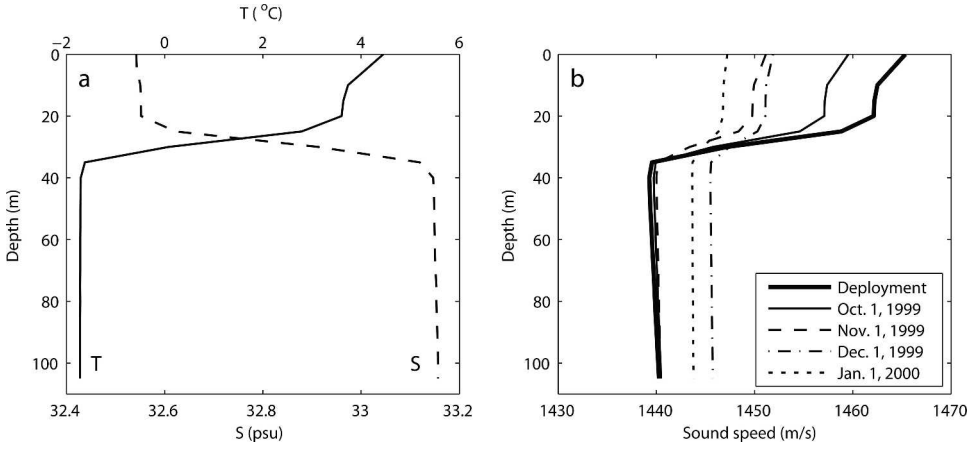

FIG. 16. Thermocline sound speed correction. (a) Vertical profiles of temperature (solid line) and salinity (dashed line) at the mooring site on 16 Sep 1999. (b) Vertical profile of sound speed calculated from the temperature and salinity data for 16 Sep 1999 (thick line) and sound speed profiles inferred using thermocline correction (thin solid and dashed lines). See text for details.

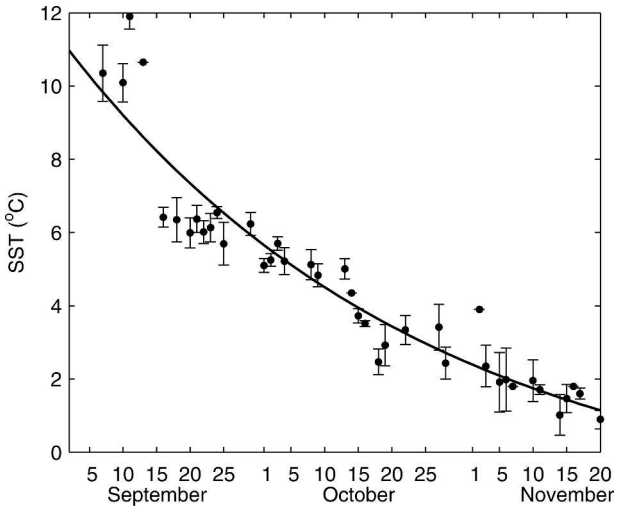

FIG. 17. Surface temperature calibration. Average AVHRR sea surface temperature within 20-km radius around the mooring site (dots) and 1 std dev (error bars) are shown. Solid line shows an exponential fit to this data.

case the sound speed variation with depth is known, c_{eff} can be obtained with good accuracy.

3) BEAMWIDTH CORRECTION

As was shown in section 3a(1), the finite width of an ADCP beam leads to the decrease in the effective beam angle and, consequently, to a negative bias in surface range estimate. This bias was corrected by accounting for the difference between the effective and nominal beam angles θ_{eff} and θ_0:

$$h_b = \frac{\cos\theta_{\text{eff}}}{\cos\theta_0} h_c, \tag{15}$$

where h_c is the surface range corrected for sound speed as described in the previous section, h_b is the range estimate additionally corrected for the beamwidth bias. For OW conditions, θ_{eff} is estimated using the model described in section 3a(1). No in situ wind measurements were available for our experiment. Satellite scatterometer observations were considered as a potential source of wind data. The QuickSCAT wind data generally agreed with the NCEP reanalysis record for the mooring locations (not shown), but had significant gaps of coverage. Consequently, the 4-times-daily NCEP wind data were used, even though such a dataset is not well suited for characterization of local sea surface roughness. The same algorithm was used to compute θ_{eff} for IC conditions, but a constant $W = 10\ \text{m s}^{-1}$ was used to approximate the roughness of new ice. Computed values of θ_{eff} that are used for the beamwidth correction are shown in Fig. 19. The mean effective beam angle was 19.2° during in autumn (September–December) when the average wind speed was 8 m s^{-1}. During the spring OW period (May–June), the mean value of θ_{eff} was slightly lower (19.0°) because of the weaker winds (5 m s^{-1}). During the ice-covered period the effective beam angle was set to 19.43°.

4) ADCP TILT, MISALIGNMENT, AND INSTRUMENT OFFSET CORRECTIONS

The distances to the surface measured by four beams may be different because of the instrument tilt. The RDI ADCPs have pitch and roll sensors, which theoretically can be used to correct for such tilt. In practice, however, the accuracy of these sensors is insufficient. We used the distances to the open-water surface h_i ($i = 1, \ldots, 4$), obtained using the WT method for each of the four ADCP beams, to infer the actual instrument roll φ_r and pitch φ_p as follows:

$$\varphi_r = \arctan\left(\frac{h_1 - h_2}{h_1 + h_2}\right) / \tan\theta_0;$$

$$\varphi_p = \arctan\left(\frac{h_4 - h_3}{h_4 + h_3}\right) / \tan\theta_0, \tag{16}$$

where θ_0 is the nominal angle of the ADCP beams to the vertical ($\theta_0 = 20°$ for the RDI Workhorse instruments we used). Here we use the convention of the roll angle being positive when transducer 2 is higher than transducer 1, and the pitch angle being positive when transducer 3 is higher than transducer 4 (Gordon 1996). For an ADCP mounted on a stable platform, such as the one used in our installation, φ_r and φ_p remain constant throughout the deployment, and can be determined with high accuracy by averaging a large number of estimates (16). After the attitude angles are determined, the ranges estimated using both the BT and WT should be updated as follows:

$$h_{1\varphi} = h_1 \frac{\cos(\theta_0 + \varphi_r)}{\cos\theta_0}; h_{2\varphi} = h_2 \frac{\cos(\theta_0 - \varphi_r)}{\cos\theta_0};$$

$$h_{3\varphi} = h_3 \frac{\cos(\theta_0 - \varphi_p)}{\cos\theta_0}; h_{4\varphi} = h_4 \frac{\cos(\theta_0 + \varphi_p)}{\cos\theta_0}. \tag{17}$$

Range estimates h_i, used in (16) and (17), should already be corrected for signal preprocessing, sound speed variation, and finite beamwidth biases using (12) and (15), but the subscript "b" has been omitted for brevity.

Mean values of φ_r and φ_p that are inferred for the ice-free period were 0.63 ± 0.10° and 0.27 ± 0.08°, correspondingly. For the comparison, roll and pitch

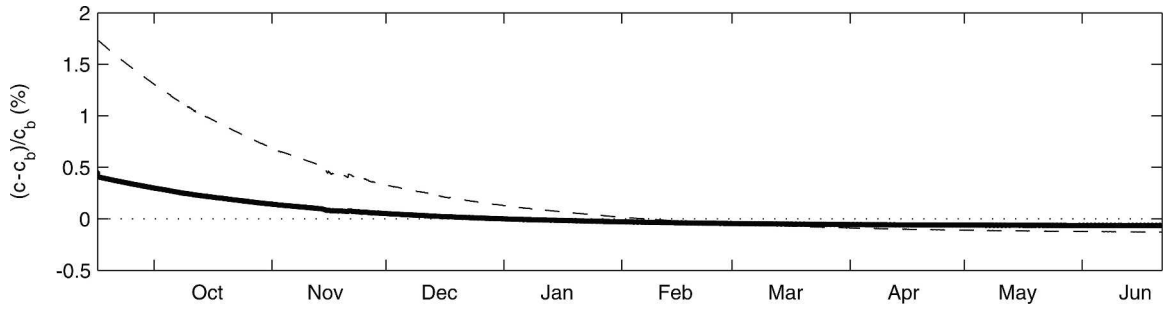

FIG. 18. Deviation of the effective sound speed c_{eff} (solid line) and its upper bound, given by the surface sound speed c_s (dashed line), from the bottom value c_b.

values that are reported by ADCP sensors were 1.03 ± 0.01° and 0.19 ± 0.01°.

If the geometry of the instrument was perfect, all of the corrected range estimates $h_{i\varphi}$ would be equal, on average. In our installation, however, mean OW values of $h_{1\varphi}$ and $h_{2\varphi}$ differed from the mean values of $h_{3\varphi}$ and $h_{4\varphi}$ by 14 cm, which is a statistically significant difference at a confidence level close to 100%. Consequently, we suspect that the transducer head of our instrument was slightly misaligned. A beam transformation matrix that is stored in the instrument's memory is supposed to reflect such misalignment; however, the matrix recorded in the log files did not show any deviations from perfect configuration.

Range corrections resulting from the beam misalignment can be obtained in a procedure similar to the one used to determine the pitch and roll angles above. We assume that the "true" range estimates h_i^* for the ith beam are related to the tilt-corrected ranges $h_{i\varphi}$ as

$$h_i^* = Q_i h_{i\varphi}, \tag{18}$$

where Q_i are correction coefficients, such that all $\langle h_i^* \rangle$ are equal to each other. (Angled brackets indicate averaging over a clear OW period when the surface is more likely to be flat.) The Q_i are found by minimization of the sum of squares of mutual differences

$$F = \sum_{i,j} \langle (h_i^* - h_j^*)^2 \rangle = \sum_{i,j} \langle (Q_i h_{i\varphi} - Q_j h_{j\varphi})^2 \rangle. \tag{19}$$

Minimization criteria

$$\frac{\partial F}{\partial Q_i} = 3Q_i \langle h_{i\varphi}^2 \rangle - \sum_j Q_j \langle h_{i\varphi} h_{j\varphi} \rangle = 0 \tag{20}$$

lead to the system of equations

$$\begin{bmatrix} 3S_{11} & -S_{12} & -S_{13} & -S_{14} \\ -S_{12} & 3S_{22} & -S_{23} & -S_{24} \\ -S_{13} & -S_{23} & 3S_{33} & -S_{34} \\ -S_{14} & -S_{24} & -S_{34} & 3S_{44} \end{bmatrix} \begin{bmatrix} Q_1 \\ Q_2 \\ Q_3 \\ Q_4 \end{bmatrix} = 0, \tag{21}$$

where $S_{ij} = \langle h_{i\varphi} h_{j\varphi} \rangle$. The system is a degenerate, so an infinite number of solutions differing by an arbitrary multiplier can be found. We additionally require all Q_i to be close to 1, thus, selecting a minimal correction. The last criterion is equivalent to minimization of

$$G = \sum_i (Q_i - 1)^2. \tag{22}$$

If Q_{i0} is an arbitrary solution of (21), then (22) is minimized by $Q_i = q\, Q_{i0}$, where q is given by

$$q = \frac{\sum_i Q_{i0}}{\sum_i {Q_{i0}}^2}. \tag{23}$$

Using (21) and (23), we found the optimal beam misalignment correction coefficients $Q_{1,2} = 0.9993$ and $Q_{3,4}$

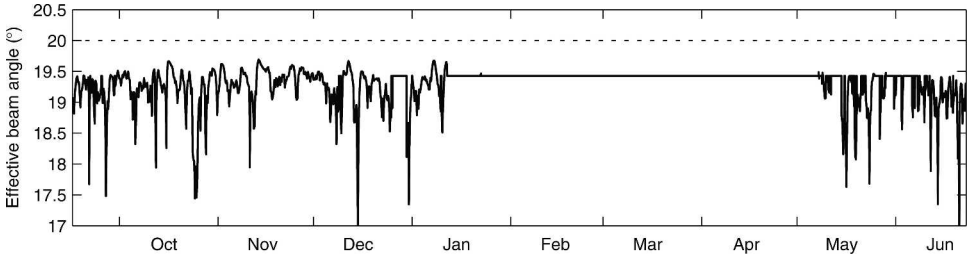

FIG. 19. Effective beam angle (solid line), computed using the model of beamwidth bias for the surface conditions estimated at the mooring site. Nominal beam angle is shown by dashed line.

TABLE 1. Magnitudes of the corrections applied to the ice draft estimated from ADCP data.

Correction	Mean offset (m)	Standard deviation (m)
Atmospheric pressure	0.01	0.07
Pressure offset	−0.07	0
Beamwidth	−0.47	0.18
Sound speed	0.03	0.13
Sensor offsets	−0.23	0
Total	−0.73	0.25
Signal preprocessing*	−0.98	0.10

* Estimated signal preprocessing bias is included for reference only; no correction for this bias was performed [see section 3a(2)].

= 1.0007. The correction is small, but it eliminates the difference between the mean OW range estimates.

It should be noted that the correction for instrument tilt and misalignment could be done in one step, using the range estimates h_{ib} that are not corrected for the tilt, instead of $h_{i\varphi}$ in (18). In that case, Q_i would also include the tilt correction. There are two reasons these corrections should be treated separately: first, the instrument may be perfectly aligned and the relatively complicated procedure of determining Q_i will not be needed; second, instrument tilt correction must be performed separately in the case of nonfixed moored installations, because no time variation of Q_i is allowed. Even though instrument tilt and beam misalignment corrections are derived using only WT data, they were also used to correct the BT range estimates.

The distances measured by the ADCP are referenced to the centers of its transducers. Because in our installation the pressure sensor was located 23 cm lower (Fig. 1b), this offset has also been taken into account.

4. Discussion

All of the corrections described above total to a mean offset of −0.73 m (Table 1, Fig. 20). The aggregate correction varies in time with a standard deviation of 0.25 m, chiefly resulting from the changes in surface roughness and atmospheric pressure. Despite all of the corrections that are applied, the resulting ice draft (or, in the OW case the difference between the distances to the surface derived from the pressure sensor and ADCP) exhibits a noticeable positive offset of 0.5–1 m at both locations (Fig. 21). This offset is likely the result of the hardware signal-preprocessing bias [section 3a(2)], as well as inaccuracies in the beamwidth and sound speed corrections. Presently, we consider this offset to be uncorrectable because of insufficient knowledge of the surface roughness, the vertical sound speed profile, and the parameters of hardware signal processing.

Similar uncorrectable offsets pose a serious problem in the analysis of specialized ice-profiling sonar data (Melling et al. 1995), because even less information about the evolution of the vertical profile of sound speed than in our case is typically available. This problem is usually circumvented by using the areas of open water passing over the mooring for establishing a "zero draft" reference. Because of the ensemble averaging, open water could only be detected if it was present throughout a substantial part of a 16-min ensemble. Subject to this constraint, no open water was observed at the location of our moorings from mid-January to May 2000. The only reliable estimate of zero draft (dashed lines in Fig. 21a) is available for the end of December, before ice cover establishment. The OW period immediately following the spring melt was also used, even though the apparent draft varied greatly during that time and the reliability of the spring estimate of zero-draft is questionable. Straight-line interpolation had to be used between these two reference periods. Ice-draft estimates at the eastern mooring appear to be more consistent with a linear approximation of zero draft (Fig. 21a).

Taking the zero-draft reference into account, typical ice drafts observed at the western and eastern moorings were 0.2–0.6 m and 0.3–0.8 m, correspondingly (Fig. 21b). Mean January–May values were 0.38 and 0.59 m, correspondingly. A maximum ice draft of 1.5 m was observed at both the western and eastern moorings just before the disappearance of the ice cover in May and June, correspondingly. Such relatively low ice thicknesses are typical for the Okhotsk Sea, especially taking into account that the moorings were located within the polynya region (Shcherbina et al. 2004; Fukamachi et al. 2003; Birch et al. 2000). Unfortunately, there are no concurrent direct observations of ice thickness in the northern Okhotsk Sea against which our estimates can be compared.

Another ice characteristic that can be derived from ADCP draft estimates is a measure of surface roughness. As mentioned earlier (see section 3), each ADCP ensemble provides four (eight in the presence of BT) estimates of ice draft. Because of the ADCP beam spreading, these estimates correspond to four points of a cross pattern on the ice surface. The horizontal separation of opposing beam footprints was 79 and 103 m for the western and eastern moorings, correspondingly. Consequently, the standard deviation of the draft estimates from each ensemble (Fig. 21c) can be used to characterize the variability of surface topography at a 50–100-m horizontal length scale. As expected, the sur-

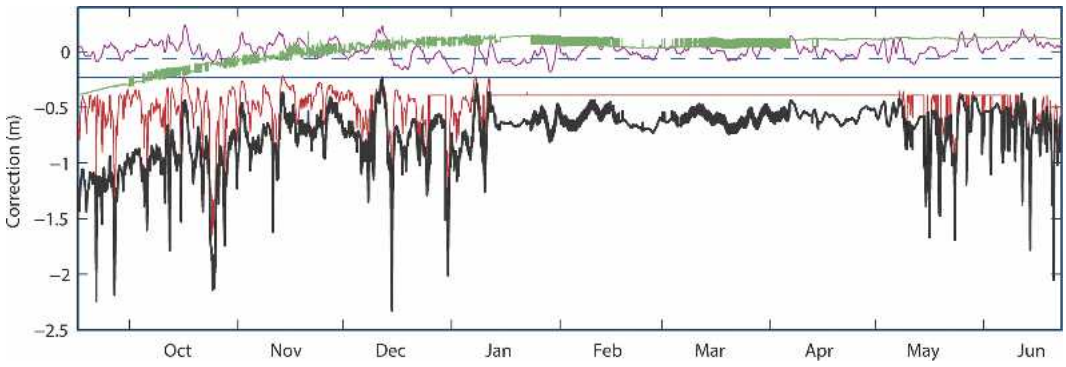

FIG. 20. Summary of corrections applied to the measured ADCP range. Corrections for atmospheric pressure (purple), sound speed (green), beamwidth (red), pressure offset (blue dashed line), and transducer offset (solid blue line) are shown, as well as the sum of all corrections (thick black line).

face of the ice is much more variable than that of the open-water surface, with a typical draft variability of 0.2–0.5 m. Early in the ice-covered period (February), the ice surface at the western site appears to be less rough than at the eastern one, consistent with the polynya conditions inshore (Shcherbina et al. 2004). Later in the season the ice roughness at the two mooring sites is comparable. The apparent roughness scale

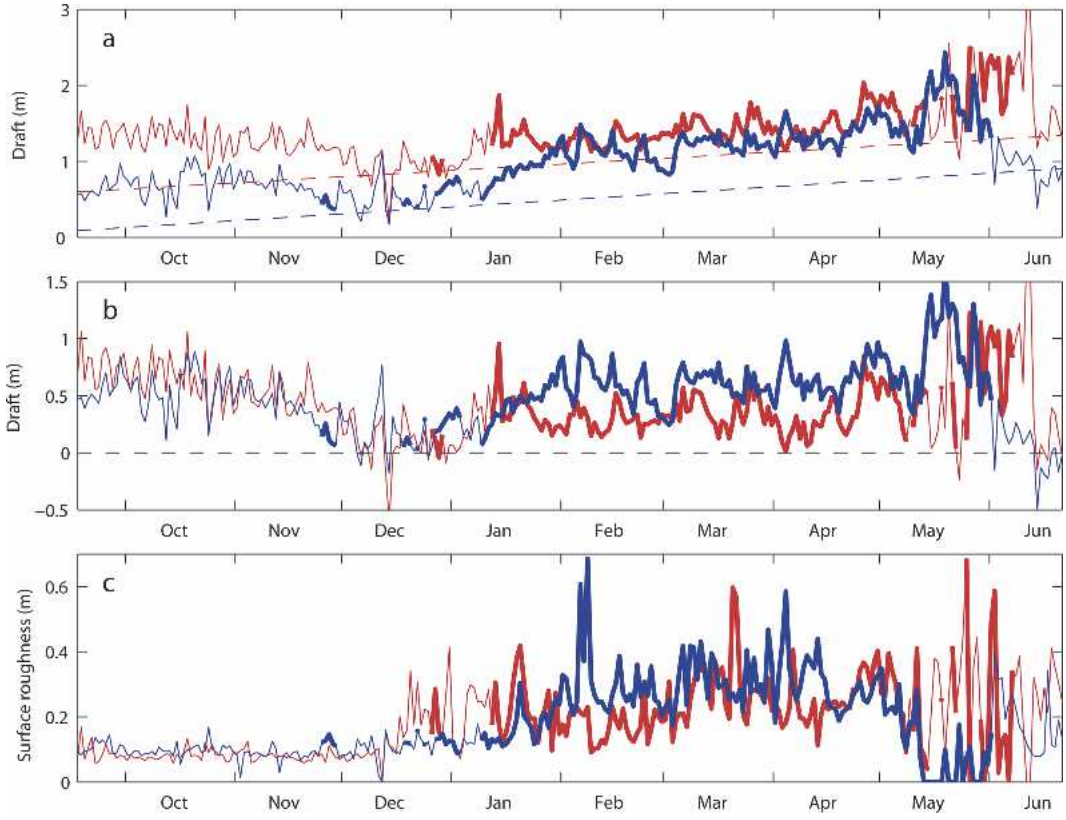

FIG. 21. (a) Raw ADCP ice draft, (b) ice draft relative to zero-draft estimate, and (c) surface roughness at the western (red line) and the eastern (blue line) moorings. Surface roughness is defied as the standard deviation of simultaneous draft estimates by four ADCP beams. Daily median estimates using all beams and both WT and BT methods (where available) are plotted in (a)–(c). Thinner lines indicate open-water conditions, determined by the echo correlation criterion. In open-water conditions ice draft is the difference between the distances to the surface derived from pressure sensor and ADCP. Dashed lines in (a) show zero-draft estimates for the two moorings.

of the open-water surface in September–December was 0.1 m at both locations. This value is comprised of sea surface height variability resulting from long-period waves and the noise in the range estimates. Consequently, we assume that the upper limit of the random error in the daily median values of ice draft that are estimated from ADCP data is on the order of 0.1 m. The additional bias is poorly known.

5. Conclusions

Ice-draft profiling with standard bottom-mounted ADCPs is possible, if bottom pressure is measured accurately at the same location. Ice draft is measured as the difference of the instrument depth derived from the pressure record and the distance to the lower ice surface measured with ADCP. The latter estimate is obtained by fitting a modified Gaussian profile to the vertical profile of the echo amplitude that exhibits a prominent peak resulting from surface reflection. Gaussian peak width and height, as well as its deviation from observed data, can be used for quality control of the range estimate. Such a "water tracking" method provides four estimates of distance to the surface per ensemble (for four-beam instruments). These estimates are inherently noisy, and need to be filtered for incorrectly detected peak locations. Additionally, corrections for atmospheric pressure, sound speed variation, finite beamwidth, instrument tilt, beam misalignment, and vertical sensor offset need to be applied. Instrument tilt and beam misalignment corrections can be determined using the water-tracking results during the open-water period. On the other hand, atmospheric pressure, sound speed, and beamwidth corrections need to be determined based on external data. This class of corrections poses a significant challenge, because their effect on the draft estimate is most pronounced (adding up to over 1.5 m in our experiment), while the external parameters that are used to derive these corrections are poorly known [see sections 3e(2) and 3e(3)]. The resolution of the final draft estimate is on the order of 0.1 m, but large unexplained positive biases exist in both of our datasets. Hardware signal processing may be potentially responsible for a large part of this bias. The exact value of the signal processing offset is difficult to obtain because of insufficient information regarding the filtering procedure. The relative importance of such a bias is expected to be less in the regions of thicker ice cover.

Based on the present analysis of the factors contributing to the errors and biases in estimating ice draft from an ADCP, the following recommendations can be offered for future experiments intending to use moored ADCPs for ice profiling:

1) The relatively wide sloping beam of an ADCP is a handicap for ice profiling, because the resulting bias is large and variable. Better understanding of the influence of surface roughness on the shape and location of the surface echo amplitude peak, as well as the better parameterization of such roughness, is necessary for reliable draft estimation.
2) The effect of hardware signal preprocessing may be large (on the order of 1 m), but its exact magnitude and dependence on surface conditions are unknown. Further investigation of the ADCP hardware is necessary to accurately correct for such an effect.
3) Ensemble averaging of the ADCP echo signal leads to a widening of the surface peak. The resulting shape depends on the probability distribution of ice draft over the ensemble duration. Consequently, only an ensemble average of ice draft can be recovered from the recorded data. If higher temporal (and, hence, spatial) resolution of ice draft is required, burst ADCP sampling should be employed.
4) The bottom tracking (BT) mode is not necessary for ice profiling, because water tracking (WT) is capable of measuring the distance to the surface with better accuracy.
5) The vertical bin size of 4 m used in our installation resulted in a surface echo amplitude peak spanning about 5–10 bins, which is sufficient for modified Gaussian profile fitting. However, a higher vertical resolution can greatly increase the reliability of such a fit and the overall accuracy of the method. Data storage constraints, which typically limit the resolution of long-term deployments, including our case, are becoming progressively less important in modern instruments.
6) An accurate surface pressure record close to the ADCP is greatly preferred. In the absence of such a record (as in the case of our experiment), large-scale reanalysis pressure data may be used for atmospheric pressure correction. However, the effects of such substitution are difficult to predict. In either case, extending the mooring pressure record several days before the deployment and after the recovery allows the surface pressure offset to be determined [see section 3e(1)].
7) As much knowledge of the evolution of the vertical sound speed profile should be obtained to enable accurate draft correction, especially in regions of unbroken ice cover.
8) The same technique of ice-draft profiling is applicable to moored (off bottom) ADCP installations, as well. However, the mooring motion leads to further complications. In particular, the accuracy of ADCP pitch and roll sensors becomes crucial, be-

cause the tilt corrections [section 3e(4)] are less reliable for varying attitude angles. Additionally, the in situ pressure sensor must be placed as close as possible to the ADCP on the mooring line, which may be technically challenging.

Incorporating a dedicated ice profiler into an experiment can potentially be infeasible or impractical, especially because it may require the installation of two separate moorings to avoid interference between the IPS and ADCP systems. With the use of correction procedures outlined in this study, ice-draft profiling can be expected to augment any moored ADCP observations in high-latitude conditions with little or no additional cost. Future experiments designed with the ADCP ice profiling in mind should, however, address the weaknesses of this procedure by following the above recommendations. In that case, the accuracy of ice profiling can be potentially improved over the present 10-cm (0.1% of water depth) baseline.

Acknowledgments. This work was supported through the National Science Foundation OCE-9811958 and by Hokkaido University (ship support). Technical support was provided by the Oceanographic Data Facility and the Instrument Development Group at Scripps Institution of Oceanography (SIO), and by the captain and crew of the R/V *Professor Khromov*. We thank Martin Visbeck, Peter Spain, and Steve Maier for stimulating discussion.

REFERENCES

Birch, R., D. Fissel, H. Melling, K. Vaudrey, K. Schaudt, J. Heideman, and W. Lamb, 2000: Ice-profiling sonar. *Sea Technol.,* **41,** 48–52.

Chapman, R. P., and H. D. Scott, 1964a: Backscattering strength of young sea ice. *J. Acoust. Soc. Amer.,* **36,** 2417–2418.

——, and ——, 1964b: Surface backscattering strengths measured over an extended range of frequencies and grazing angles. *J. Acoust. Soc. Amer.,* **36,** 1735–1737.

Cox, C., and W. Munk, 1954: Measurement of the roughness of the sea surface from photographs of the sun's glitter. *J. Opt. Soc. Amer.,* **44,** 838–850.

Fukamachi, Y., G. Mizuta, K. I. Ohshima, H. Melling, D. Fissel, and M. Wakatsuchi, 2003: Variability of sea-ice draft off Hokkaido in the Sea of Okhotsk revealed by a moored ice-profiling sonar in winter of 1999. *Geophys. Res. Lett.,* **30,** 1376, doi:10.1029/2002GL016197.

Gordon, R. L., 1996: *Acoustic Doppler Current Profilers Principles of Operation: A Practical Primer.* RD Instruments, 54 pp.

Macpherson, J. D., 1963: The effect of ice on long range underwater sound propagation. *J. Brit. IRE,* **26,** 293–297.

Melling, H., 1998: Sound scattering from sea ice: Aspects relevant to ice-draft profiling by sonar. *J. Atmos. Oceanic Technol.,* **15,** 1023–1034.

——, P. Johnston, and D. Riedel, 1995: Measurements of the underside topography of sea ice by moored subsea sonar. *J. Atmos. Oceanic Technol.,* **12,** 589–602.

Shcherbina, A. Y., L. D. Talley, and D. L. Rudnick, 2004: Dense water formation on the northwestern shelf of the Okhotsk Sea: 1. Direct observations of brine rejection. *J. Geophys. Res.,* **109,** C09S08, doi:10.1029/2003JC002196.

Strass, V., 1998: Measuring sea ice draft and coverage with moored upward looking sonars. *Deep-Sea Res.,* **45,** 795–818.

Urick, R. J., 1956: The process of sound scattering at the ocean surface and bottom. *J. Mar. Res.,* **15,** 134–148.

——, 1975: *Principles of Underwater Sound*. McGraw-Hill, 384 pp.

Visbeck, M., 2002: Deep velocity profiling using lowered acoustic Doppler current profilers: Bottom track and inverse solutions. *J. Atmos. Oceanic Technol.,* **19,** 794–807.

——, and J. Fischer, 1995: Sea surface conditions remotely sensed by upward-looking ADCPs. *J. Atmos. Oceanic Technol.,* **12,** 141–149.